Vaccine: X 18 (2024) 100474

Contents lists available at ScienceDirect

Vaccine: X

journal homepage: www.elsevier.com/locate/jvacx

Efficient and scalable clarification of Orf virus from HEK suspension for vaccine development

Felix Pagallies [a,1], Jennifer J. Labisch [b,1], Malgorzata Wronska [a,c], Karl Pflanz [b], Ralf Amann [a,c,*]

[a] Department of Immunology, University of Tuebingen, Auf der Morgenstelle 15, 72076 Tübingen, Germany
[b] Lab Essentials Applications Development, Sartorius, Otto-Brenner-Straße 20, 37079 Göttingen, Germany
[c] PRiME Vector Technologies, Herrenberger Straße 24, 72070 Tübingen, Germany

ARTICLE INFO

Keywords:
Harvest
Clarification
Parapoxvirus Orf
Nuclease treatment
Multi-parallel filtration
Filter screening

ABSTRACT

The Orf virus (ORFV) is a promising vector platform for the generation of vaccines against infectious diseases and cancer, highlighted by its progression to clinical testing phases. One of the critical steps during GMP manufacturing is the clarification of crude harvest because of the enveloped nature and large size of ORFV. This study presents the first description of ORFV clarification process from a HEK suspension batch process. We examined various filter materials, membrane pore sizes, harvest timings, and nuclease treatments. Employing the Ambr® crossflow system for high-throughput, small-volume experiments, we identified polypropylene-based Sartopure® PP3 filters as ideal. These filters, used in two consecutive stages with reducing pore sizes, significantly enhanced ORFV recovery and addressed scalability challenges. Moreover, we demonstrated that the time of harvest and the use of a nuclease play a decisive role to increase ORFV yields. With these findings, we were able to establish an efficient and scalable clarification process of ORFV derived from a suspension production process, essential for advancing ORFV vaccine manufacturing.

1. Introduction

The Orf virus, belonging to the genus Parapoxvirus of the Poxviridae family, is a viral pathogen that in its wild-type form affects predominantly sheep and goats known as Orf disease [1,2]. ORFV is an ovoid-shaped, enveloped virus with a length of approximately 220–300 nm and a width of 140–200 nm [3], characterized by a spirally tubular structure on its surface [4]. The viral genome comprises a linear double-stranded DNA of approximately 140 kb [5] and representing a potent platform for viral vector vaccine development. The ORFV D1701-VrV is a highly attenuated, non-pathogenic strain generated by the deletion of several ORFV virulence genes [6]. The key advantages of this vector is the very restricted host range, absence of systemic spread, the large genomic size allowing integration of multiple transgenes, and the exclusive cytoplasmatic gene expression [6,7]. Furthermore, it was demonstrated that the D1701-VrV strain induces strong transgene-specific immune response without triggering anti-vector immunity allowing repeated immunizations resulting in fast and strong adaptive immune responses [8].

The ORFV D1701-VrV recombinants have already been shown to mediate immunity against different viral infections like dengue virus [9], influenza A virus [10], rabies virus [6], pseudorabies virus [11–13], classical swine fever [14], rabbit hemorrhagic disease virus [15], and borna disease virus [16]. ORFV has also been used for oncolytic therapy [17] and as a therapeutic vaccine for virus-induced tumors [18]. More recently, the ORFV vector platform was used to develop a Sars-Cov-2 vaccine candidate, which is currently undergoing Phase I clinical trials [19].

With the growing number of ORFV technologies and applications with potential therapeutic or vaccine candidates entering clinical phases, the demand for scalable production and downstream processing (DSP) methods for ORFV is increasing. However, the available literature on suitable upstream and downstream processing methods for ORFV remains sparse.

The production of ORFV D1701-VrV was initially based on adherent Vero cell culture [20]. The harvest protocols include centrifugation steps, cell lysis by several freeze–thaw cycles and sonication, followed by depth filtration. The purification was traditionally performed by ultracentrifugation and polyethylene glycol (PEG) precipitation [21]. Although effective in a small scale, these purification methods lack

* Corresponding author at: Department of Immunology, University of Tuebingen, Auf der Morgenstelle 15, 72076 Tübingen, Germany.
E-mail address: Ralf.Amann@ifiz.uni-tuebingen.de (R. Amann).
[1] Shared first authorship.

https://doi.org/10.1016/j.jvacx.2024.100474
Received 29 November 2023; Received in revised form 1 March 2024; Accepted 12 March 2024
Available online 13 March 2024

scalability. Efforts to overcome this limitation focused on identifying suitable clarification and chromatography methods [22–24]. However, these process optimizations were still based on the adherent Vero cell production process. To enable industrial-scale production of ORFV, we replaced the adherent Vero cell process by a HEK suspension process. This transition, however, introduced complications, particularly in the clarification step. These challenges were anticipated, as the clarification strategy depends on the upstream process, such as expression system, cell density and viability, and media composition. These factors determine the type and amount of impurity load. Moreover, the large macromolecular size and complex structure of the target virus pose challenges for the clarification. Despite its critical importance in influencing the efficiency of subsequent DSP steps, clarification has often been overlooked during process development, with a notable lack of detailed studies in the literature. Clarification typically involves a series of operations, namely primary and secondary clarification, aiming to remove cells, cell debris and large aggregates [25]. Given the large size of enveloped vectors, the final pore size in the secondary clarification step often uses membranes with pore sizes usually not smaller than 0.45 or 0.65 μm [26,27].

Recognizing the gap in detailed investigations into effective clarification methods for ORFV or analogous vectors, our goal was to devise a scalable clarification strategy that maximizes yield for ORFV generated in HEK cells grown in suspension. Due to the lack of comprehensive large screening studies of suitable clarification approaches for ORFV or analogous vectors, tour goal was to develop a scalable clarification strategy that maximizes yield for ORFV produced in suspension HEK cells and to improve subsequent DSP steps. This study marks the first detailed examination of the clarification process of ORFV produced by a HEK suspension batch process. We investigated various factors including different filter materials, membrane pore sizes, harvest times, and nuclease treatments, aiming to fine-tune these parameters for optimal results. Our findings have led to the establishment of an efficient and scalable clarification process for ORFV derived from a suspension production process, paving the way for improved DSP efficiency and clinical application.

2. Materials and methods

2.1. ORFV vector production

The ORFV strain D1701-V-GFP encoding the green fluorescent protein (GFP) in the vegf insertion locus [7] was produced by HEK293F viral production cells (Thermo Fisher Scientific, A35347) in a 10 L UniVessel® bioreactor (Sartorius). with the bioprocess was monitored and controlled using a BIOSTAT®-B DCU (Sartorius). The bioreactor was inoculated with 500–1000 mL of cell solution achieving an initial cell density of 7.5E+05 cells•mL^{-1}. After 24 h, when cell density reached 1.5E+06 cells•mL^{-1}, the cells were infected with a multiplicity of infection of 0.1 by adding the vector in 50 mL of medium to produce ORFV. Additionally, GlutaMAX (Thermo Fisher Scientific) was added to a final concentration of 2 mM.

2.2. Harvest and clarification

The ORFV cell culture broth (crude harvest) was harvested 72 h post-infection, undergoing a freeze–thaw cycle before filtration. Initial screening tested various filters (Cytiva, Merck, Meissner, 3M and Sartorius) for efficacy. The clarification was performed with the PendoTECH Filter Screening System (PendoTECH) using following parameters: flow rate 3.2 mL•min^{-1}, maximum pressure 1000 mbar, equilibration of filter with 100 mL of PBS buffer pH 7.2 (Thermo Fisher Scientific). Filtrations were performed until a pressure of max. 0.8 bar was reached for single filtrations and max. 1 bar for filter trains. In case of an early occurrence of visual turbidity breakthrough or if no pressure increase occurred, filtrations were stopped earlier.

After the initial filter screening, the most suitable membrane material (PP3) was further evaluated using the Ambr® crossflow system (Sartorius) in combination with the Sartocon® Slice 50 adapter (Sartorius) enabling parallelized dead-end filtrations. A scheme of the filtration setup is shown in Fig. 1.

For the clarification optimization experiment, a 6 L ORFV batch was produced and2 L of crude harvest was collected 40, 70, and 90 h (±4h for each) post-infection to determine the ideal time of harvest (TOH). Subsequently, crude harvest was aliquoted in 0.5–1 L flasks and 60 U•mL^{-1} of the nucleases M-SAN HQ or Denarase® were added together with magnesium chloride in a final concentration of 10 mM for M-SAN HQ and 2 mM for Denarase®, and incubated for 4 h at 160 rpm in a MaxQ™ 6000 shaking incubator (Thermo Fisher Scientific) at 37 °C. A non-nuclease-treated fraction served as a control. SartoScale 25 filters containing the Sartopure® PP3 membrane were used for primary (pore size of 20, 8, or 5 μm) and secondary filtration (pore size of 1.2, or 0.65 μm). The filters were equilibrated with 10 mL of LV-MAX mixed with PBS in a 1:1 ratio at a flow rate of 3 mL•min^{-1}. A flow rate of 2 mL•min^{-1} was applied for the filtration of the crude harvest material. The maximum pressure was set to 1 bar and a maximum of 100 mL was filtered.

2.3. Design of experiment for nuclease treatment optimization

A design of experiment (DoE) approach was utilized to optimize nuclease digestion focusing on five variables: i. incubation time (0.5–6 h), ii. Temperature (4, 23, 37 °C), iii. Nuclease (Denarase® (c-LEcta), M-SAN HQ, and SAN HQ (both ArcticZymes)), iv. Concentration of the nuclease (from 2 to 100 U•mL^{-1}), and v. sodium chloride (NaCl) concentration (180–480 mM). Magnesium chloride was added to achieve final concentrations of 2 mM for Denarase®, or 10 mM for M-SAN HQ, and SAN HQ, respectively. The experiments were planned as a D-optimal design (interaction model) and evaluated using the software MODDE® 13 (Sartorius) with a center point of triplicates for each nuclease at a certain condition (50 U•mL^{-1} nuclease, 3.5 h, 23 °C, 150 mM NaCl), as well as four other conditions which were run in duplicates, resulting in a total of 44 experiments This design was applied twice using different ORFV material forms: crude harvest and clarified supernatant obtained by centrifugation at 4,000× g for 15 min. Details on the experimental setup are included in Table S1.

2.4. Analytics

2.4.1. Determination of infectious ORFV titer

The infective ORFV titer was determined by quantifying GFP expressing Vero cells using flow cytometry. Each well of a 96-well plate was seeded with 40,000 Vero cells in 200 μL of DMEM supplemented with 5 % FCS. ORFV samples, diluted in a 1:4 series from 0 to 1024, were added to the cells, which were then incubated for 20 ± 2 h post-infection. Following incubation, cells were washed with PBS, detached with Trypsin/EDTA, and neutralized with DMEM plus 5 % FCS. After centrifugation, the cell pellet was resuspended in PFEA buffer, with an optional fixation step using 1 % formaldehyde in PFEA (PBS, 2 % v/v FCS, 2 mM EDTA, 0.02 % v/v sodium azide). A final wash preceded flow cytometric analysis (AttuneNxT). The infective titer, expressed in infectious units per milliliter (IU•mL^{-1}), was calculated from the percentage of GFP-positive cells, using a standard curve derived from a known ORFV standard.

2.4.2. Total dsDNA quantification

The concentration of total dsDNA was determined using the Quant-iT™ Pico-Green™ dsDNA assay (Thermo Fisher Scientific) according to the manufacturer's instructions. Standards and samples were assessed in duplicates in black 96-well microtiter plates (Nunc, Thermo Fisher Scientific). The samples were excited at 480 nm, and the fluorescence emission intensity was measured at 520 nm using an Infinite 200 PRO®

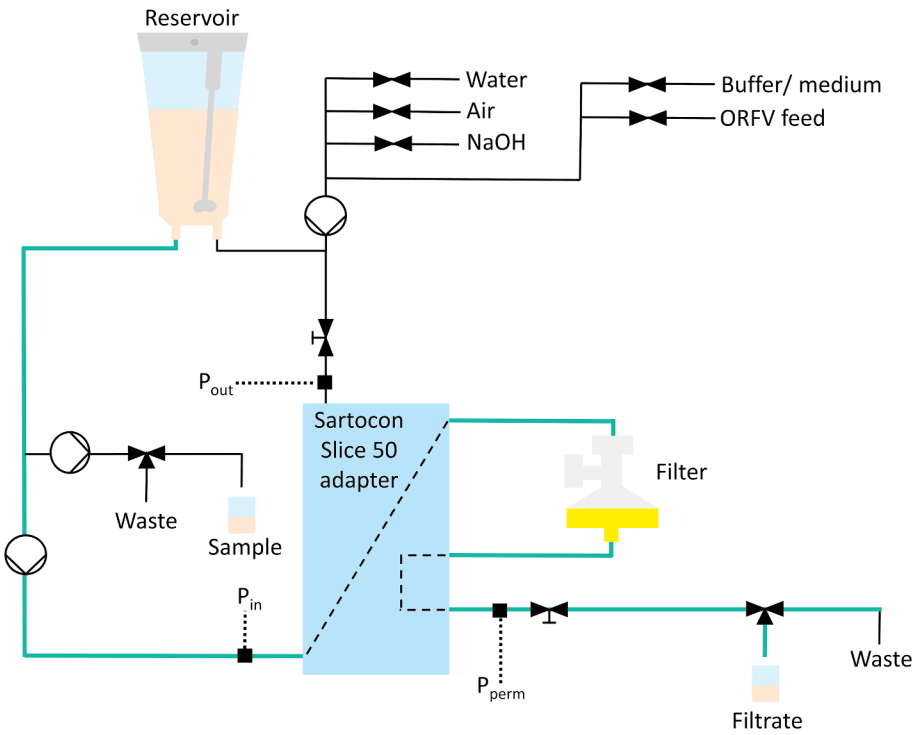

Fig. 1. Flow path scheme of the Ambr® crossflow with the Sartocon® Slice 50 adapter. The flow path used is highlighted in green. (For interpretation of the references to color in this figure legend, the reader is referred to the web version of this article.)

microplate reader (Tecan). The standard curve was fitted by linear regression.

2.4.3. Turbidity measurement

Turbidity levels before and after clarification were assessed by measuring the OD400 nm of 200 µL samples. These measurements were conducted using a clear 96-well microtiter plate and an Infinite 200 PRO® (Tecan) plate reader. Measurement was performed immediately after pipetting samples into the plate.

3. Results

3.1. Evaluation of different filter types

We evaluated various filter types and filter combinations, including depth and membrane filters from several manufacturers, for their efficiency in clarify ORFV from crude harvest that underwent a freeze–thaw cycle. The crude harvest had a cell density of 3-4E+06 cells•mL^{-1}, a cell viability of <10 %, and an ORFV titer of 1.88E+07 IU•mL^{-1}. Table 1 summarizes the performance of these filters. The depth filter trains (Seitz® filters) yielded a low ORFV recovery rate of 20–30 %, while over 80 % of the DNA amount could be removed. The Profile® Star filters achieved higher ORFV recoveries of 64–102 % while removing lower DNA amounts of 25–44 %.

To further investigate whether diatomaceous earth (DE) in depth filters affects ORFV adsorption, we analyzed virus titers across 10 filtrate fractions totaling 100 mL, using Seitz® V100P filter (without DE) and Seitz® K100P (containing DE). Interestingly, initial filtration fractions showed a decrease in ORFV titer, more so with the K100P filter, where the virus became detectable only after filtering 40 mL (Fig. S1). With increasing filtration volume, the ORFV recovery rate increased, thus indicating a saturation effect of the unspecific binding or adsorption effect.

Given their superior performance in enhancing ORFV yield, polypropylene filters were selected for was further evaluation using a new, unfrozen ORFV batch. This batch presented a cell density of 1.72E+06 cells•mL^{-1}, a cell viability of 35 %, and an ORFV titer of 6.47E+07 IU•mL^{-1} for the crude harvest and 3.17E+07 IU•mL^{-1} for the supernatant. Profile® Star and HDC® II filter trains were tested and based on the filter capacity and extrapolation, the required amount of filter capsules for scaling up to a 200 L industrial production was calculated (Table 2).

Profile Star® 10 µm reached a pressure of 1 bar after processing 77 L•m^{-2}. During the second filtration step with a 1.5 µm filter, no pressure increase was observed, and the filtration was stopped after 77 L•m^{-2} at 0.07 bar. This corresponds to a required membrane area of 3.6 m2 for the first filtration step which is equivalent to 10 × 30″ Kleenpak™ Nova capsules, 6 × 30″ Kleenpak™ Nova capsules for the second filtration step. The 20 µm HDC® II filter showed a slow gradual pressure rise teaching 0.2 bar after 128 L•m^{-2}. The second filtration step with the 10 µm HDC® II showed a similar pattern reaching 0.14 bar after 125 L•m^{-2}. The final filtration step with 2.5 µm showed a sharp pressure rise, indicating a filter capacity of 8 L•m^{-2}. The required membrane area of this last filtration step of 21 m2 would correspond to 8x 30″ Kleenpak™ Nova capsules. ORFV yield was about 75 % with the Profile® Star filter train and about 61 % with the HDC® II filter train (20 and 10 µm), while nearly all ORFV was lost with the final 2.5 µm filter.

Given the insufficient filter capacity for scaling up to 200 L, alternative polypropylene filters were considered to enhance both ORFV yield and DNA removal efficiency. Thus, four other filter combinations for primary and secondary clarification were evaluated from different manufacturers, which are listed in Table 3.

The Zeta Plus™ and the Sartoclear® DL90 resulted in ORFV recovery less than 10 % after primary clarification, and thus not suited for ORF clarification. The 5 µm ALpHA® filter achieved an infectious ORFV recovery of 97 % after primary clarification but encountered immediate blocking during secondary clarification with the 0.6 µm filter, leading to total ORFV loss. The Millistak+® µPod® filter, with a pore size range of 0.6–0.9 µm, achieved 41 % recovery after primary clarification. However, recovery rates dropped to 2 % or less during secondary clarification for all tested filters. This suggests that while the Millistak+® µPod® may suffice for single step filtration, it fails to reach the target recovery

Table 1
Tested filters of initial filter screening with respective ORFV yield. Abbreviations: polypropylene - PP, polyether sulfone - PES, polyvinylidene fluoride - PVDF, diatomaceous earth - DE.

Filter combinations	Filter material	Pore size (μm)	Effective filter areas (cm^2)	ORFV yield (%)	DNA removal (%)
Seitz® P900; V100P; Bio20	P900: cellulose, perlite, DE, resin; V100P: cellulose, perlite, resin; Bio20: cellulose, resin	8–20; 2–4; 0.4–0.8	22 each	31.45	85.73
Seitz® PDP8; V100P; Bio20	PDP8: cellulose, perlite, DE, resin; V100P: cellulose, perlite, resin; Bio20: cellulose, resin	6–30; 2–4; 0.4–0.8	22 each	31.22	83.48
Seitz® PDK7; V100; Bio20	PDK7: cellulose, perlite, DE, resin; V100P: cellulose, perlite, resin; Bio20: cellulose, resin	4–20; 2–4; 0.4–0.8	22 each	19.56	95.28
Profile® Star	PP	20	90	87.37	24.81
Profile® Star; Fluorodyne® II DBL	PP; PVDF	20; 3; 0.45	90; 13	64.23	44.29
Profile® Star; HDC® II	PP	20; 3; 0.6	90; 13	102.38	44.42

Table 2
Tested filters for ORFV clarification with respective ORFV yield and dimensioning of required filter capsules for a 200 L industrial batch at max. 0.8 bar and 25 % safety in 2–4 h. Abbreviations: polypropylene - PP.

Filter combinations	Filter material	Pore size (μm)	Effective filter areas (cm^2)	ORFV yield (%)	Required material for 200 L batch (m^2)
Profile® Star	PP	10; 1.5	90 each	74.71	3.6; 2.16
HDC® II	PP	20; 10;	13 each	61.04	1.5;1.5
HDC® II	PP	20; 10; 2.5	13 each	0.28	1.5;1.5; 21.1

goal of >80 %.

3.2. Nuclease treatment optimization

Our initial findings indicated a trade-off between ORFV recovery and DNA removal: filters with better ORFV recovery were less efficient in DNA clearance, suggesting a competition between virus retention and DNA elimination. Consequently, refining DNA digestion before filtration appears essential for improving the purification process.

To address this, we adopted a DoE approach for nuclease digestion optimization. An ORFV batch produced in a Biostat-B DCU 5L Univessel®. The crude harvest had a cell density of about 5.09E+06 cells•mL^{-1} And underwent one freeze–thaw cycle. The nuclease treatment optimization was performed on both, the crude harvest and the supernatant obtained by centrifugation, with pH levels maintained between 7.8 and 8.2.

The analysis clarified that the total DNA content in the crude harvest, encompassing both supernatant and cell-associated DNA. Consequently, DNA concentrations in the supernatant are typically lower. Across all nucleases tested, weather applied to crude harvest or supernatant sample, DNA concentration decreases with increasing nuclease concentration up to an optimal range of approximately 60–80 U•mL^{-1} (Fig. S2).

Fig. 2 presents a 4D contour plot illustrating comparable outcomes for both, the crude harvest and supernatant. Among the three nucleases tested under different conditions for the crude harvest, M-SAN HQ resulted in the lowest DNA concentrations and performed best, followed by the SAN HQ. Denarase® results in the highest DNA concentration for both, crude harvest, and supernatant. The addition of salt did not contribute to reducing DNA concentration (data not shown), leading to the exclusion of this factor in the DoE analysis. Higher incubation temperatures and extended incubation times resulted in lower DNA concentrations. Although nuclease treatment sometimes increased the ORFV titer of the crude harvest, these changes fell within the error margin of the titer quantification assay. ORFV titers in the supernatant were unaffected across all tested nucleases or parameters (data not shown).

In selecting the optimal conditions for DNA digestion, our goal was to minimize both time and nuclease concentration to reduce process time and costs. The nuclease M-SAN HQ emerged superior for further treatment before clarification with 60–75 U•mL^{-1}, at 37 °C for 4 h reducing DNA concentration to <500 ng•mL^{-1}.

3.3. Filter screening with nuclease treatment

For comprehensive filter screening, two 6 L ORFV batches were produced, examining three different harvesting times to test all filters. Fig. 3 shows the cell concentration, viability, infection rate and ORFV titer over the cultivation period. Cell count peaked at 2.3–3.3E+06 cells•mL^{-1} around 65 h post-infection without increase further. Viability started to decline slowly post-infection and dropped rapidly after 40 h. The highest infection rates were observed after 21–43 h with 75–90 % and decreased thereafter due to diminishing cell viability and the corresponding decrease in the GFP signal from infected cells. ORFV titer increased until approximately 40 h after infection and did not increase further thereafter. Harvests were done at 40, 70, and 90 h (±4h for each) post-infection (TOH (time of harvest) 1, 2, or 3) and subjected to filtration with or without nuclease digestion using M-SAN HQ (Fig. 4) or Denarase® (Fig. S3).

Without nuclease digestion, ORFV yields ranged from 17 to 37 % for TOH 1 and increased at subsequent TOH 2 and TOH 3 as indicated by higher titers (Fig. 4A, Fig. S4A). C Yields generally improved with nuclease treatment. M-SAN HQ significantly increased the yield of TOH 1 to 48 %–81 %. The highest yields were achieved at TOH 2, followed by TOH 3. Interestingly, a final membrane pore size of 0.65 μm resulted in higher ORFV recovery than a 1.2 μm pore size (Figs. 4B and S4B). Utilizing broader primary filters (20 or 8 μm) resulted in a higher ORFV recovery compared with the 5 μm filter, likely due to their ability to allow more ORFV particles, potentially in aggregates or attached to cell fragments, to pass through the filters.

Fig. 4C and 4D display the turbidity results from the clarification screening, highlighting its importance as an indicator of contaminant removal efficiency in filtration processes. As expected, the largest membrane pore size of 20 μm resulted in the highest turbidity after filtration, as large contaminants were still able to pass the membrane.

Table 3
Other filters tested for ORFV clarification. The clarified material of the primary clarification was pooled and then used for the secondary clarification.

	Filter	Manufacturer	Filter material	Pore size (µm)	Effective filter areas (cm^2)	ORFV yield (%)
Primary clarification	Millistak+® µPod® D0HC	Merck	Cellulose, inorganic filter aid	0.6–0.9	23	41
	ALpHA® MF-grade 50 mm capsule	Meissner	Polypropylene	5	19.6	97
	Zeta Plus™ BC series	3M	Cellulose	0.55–5	25	7
	Sartoclear® DL90 depth filter	Sartorius	Cellulose, inorganic filter aid	2–20	25	4
Secondary clarification	Millistak+® µPod® B1HC	Merck	Cellulose, inorganic filter aid	0.01–0.7	23	1
	ALpHA® MF-grade 50 mm capsule	Meissner	Polypropylene	0.6	19.6	0
	Zeta Plus™ BC series	3M	Cellulose	0.2–3	25	2
	Sartoclear® DL20 depth filter	Sartorius	Cellulose, inorganic filter aid	0.8-0.4	25	0

The 8 and 5 µm filtrations had a lower turbidity level. Implementing a secondary filtration step with finer membranes further reduced turbidity by capturing smaller contaminants. The turbidity was in general a little bit lower with prior nuclease treatment, which was more pronounced for the TOH 1 and 2. The turbidity of the filtered material increased for later TOH, correlating with an increase in the turbidity of the cell culture broth prior to filtration.

Fig. 4E shows that using a dual filter system, without prior nuclease treatment, reduces the dsDNA concentration in the filtrate to below 2000 ng•mL^{-1}. Conversely, a single, larger pore filter resulted in higher final dsDNA concentrations of up to 6000 ng•mL^{-1}. Treating the harvest with M-SAN HQ before a two-stage filtration process achieves dsDNA concentrations below 1000 ng•mL^{-1}. The lowest dsDNA concentrations, 16 ng•mL^{-1} at TOH 3, was obtained using a combination of M-SAN HQ and the 5 + 1.2 µm filter. In general, a consistent trend of decreasing DNA concentration in the filtrate with decreasing membrane pore size was observed.

The filter capacities of the Sartopure® PP3 filters were determined based on the maximum pressure reached. If the intended maximum pressure of 1 bar was not reached due to limited feed material, filtration was stopped prematurely, and the pressure at cessation was recorded to estimate the filters minimum operational capacity (Table 4).

Filtrations involving a single step frequently hit this maximum pressure, particularly as pore size diminished, leading to increased likelihood of membrane clogging and reduced filter capacity. This trend was consistent across all TOH, with capacities for 8 and 5 µm filters accurately determined. Filter capacity tended to decline for later TOH, attributed to reduced cell viability, resulting in more cell debris and contaminants. A difference in filter capacity between untreated feed material and feed material treated with M-SAN HQ was not apparent.

During secondary clarification, pressure increased more slowly, often not reaching the maximum pressure required to calculate the capacity. This limitation, caused by restricted feed material volume, meant not every filter combination were tested to 1 bar, thus the indicated capacity represents the minimum values and the maximum capacity for these filtrations is only a rough estimate. However, it is evident that primary filtration effectively removed larger impurities thereby reducing the load on secondary filter and enhancing their capacity.

4. Discussion

4.1. Evaluation of different filter types

ORFV has emerged as a compelling candidate for vaccine development against infectious diseases and cancers, reaching clinical trial stages where efficient and cost-effective Good Manufacturing Practice (GMP) production at large-scale is paramount. One of the critical steps during GMP manufacturing is the clarification of crude harvest because of the enveloped nature and large size of ORFV. The process of virus recovery and purification from production cell lines involves critical steps that impact the overall yield and quality of the viral vectors. The enveloped nature of ORFV adds complexity to its recovery from host cells. Unlike retroviral vectors that bud from the host cell membrane acquiring their envelope [28], poxviruses like ORFV are predominantly intracellular, with a fraction becoming enveloped through more complex cellular pathways, involving the endoplasmic reticulum and the *trans*-Golgi network [29,30]. This biological nuance necessitates methods like freeze–thaw cycles to disrupt cells and release the intracellular virions, a method that, while effective in laboratory scales, poses scalability and practicality issues for large-scale vaccine production.

The initial filter material screening revealed promising DNA removal with Seitz® depth filters, but ORFV recovery was low, possibly due to DE adsorption until saturation. The effect of adsorption of viral vectors to DE, was previously discussed for lentiviral vectors and adeno-associated vectors [31,32]. As these depth filters were initially developed for monoclonal antibody clarification of high cell density CHO processes [33], the DE amount is likely too high for our application. Also, other depth filters without DE adsorbed ORFV particles, as their concentrations slowly increased with increasing filtration volume.

Through the screening of different filter materials, we identified polypropylene-based filters as the optimal choice for ORFV clarification, achieving significant vector recovery alongside effective removal of cells and cell debris. Polypropylene is an inert material [25] and was reported by Gränicher et al. as effective for clarifying a Modified Vaccinia Ankara virus (MVA) produced in a suspension cell line. Similar to ORFV, MVA is a large-sized member of the Poxvirus family that strictly replicates within the cytoplasm. In their study, a Sartopure® PP3 0.45 µm filter achieved 60 % and 80 % recovery rates for batch and perfusion processes, respectively [27]. We further evaluated the polypropylene-based Profile® Star and HDC® II filter trains for potential scale-up to 200 L which would resulting in approx. 2 million doses. However, our analysis of filter capacity and subsequent extrapolation revealed that achieving the desired scale with these specific filters can technically very challenging and would not be straightforward.

A subsequent screening of filters from different materials and manufacturers (referenced in Table 3) confirmed that polypropylene is a promising filter material in delivering high ORFV recovery during primary clarification. However, challenges in secondary clarification were highlighted by significant filter capacity limitations, rendering the filtration process impractical for large-scale processes. This screening revealed that cellulose filters and those containing filter aids were not suited for ORFV clarification due to poor recoveries. Despite these challenges, polypropylene filters in general appeared promising, suggesting that with enhancements in capacity, they could become the

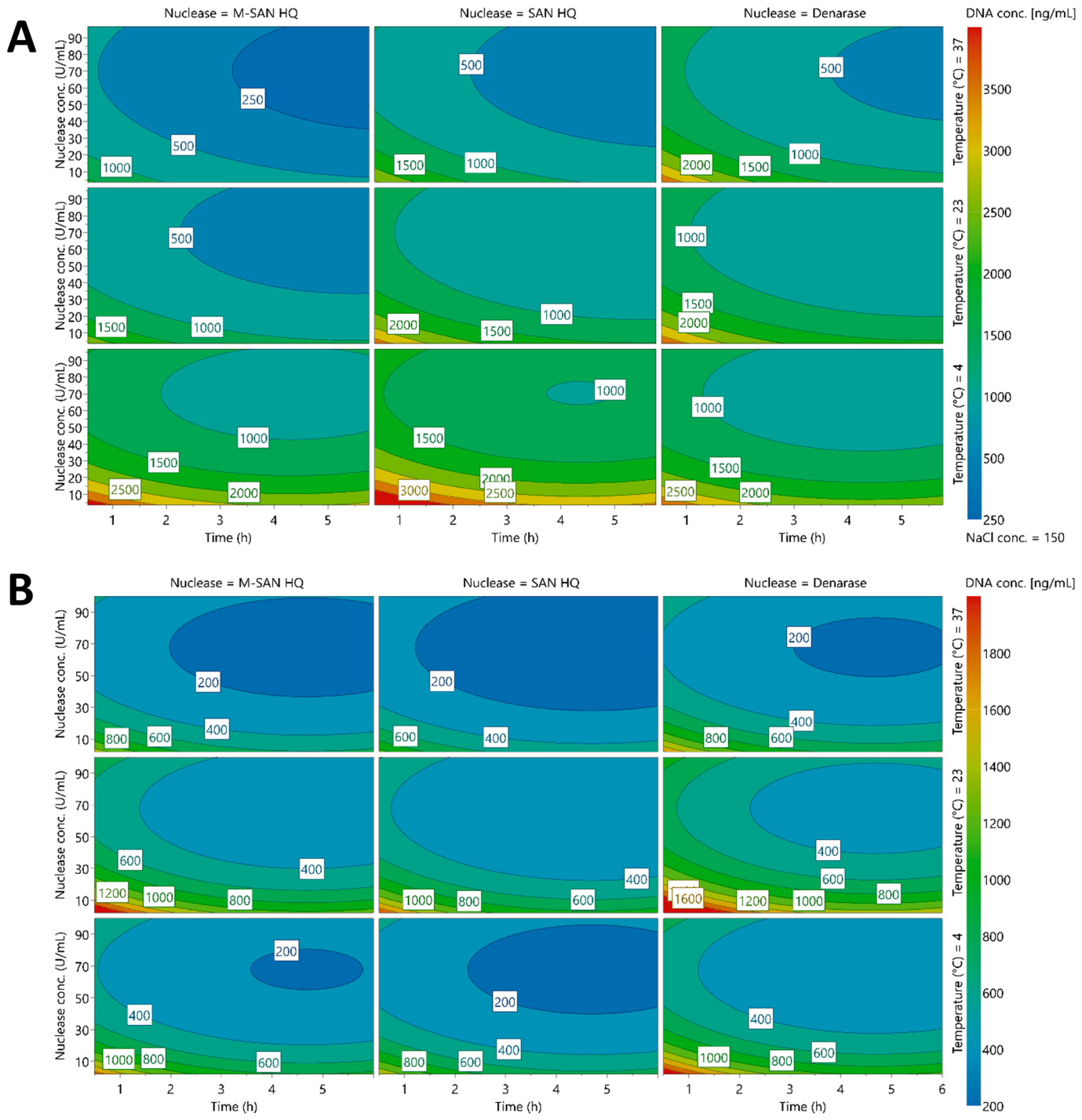

Fig. 2. 4D contour plot of the DNA concentrations in ng•mL^{-1} after nuclease digestion. Treated material was (A) crude harvest and (B) supernatant with M-SAN HQ (first column), SAN HQ (second column), and Denarase® (third column) in dependence of the factors incubation time in h (x-axis), nuclease concentration in U•mL^{-1} (y-axis) and incubation temperature (first row 4 °C, second row, 23 °C, third row 37 °C).

preferred filter material of choice for further experiments.

4.2. Nuclease treatment optimization

Nucleic acid impurities derive mainly from host cell DNA). According to European Pharmacopeia [34]approved vector-based vaccines should reduce the size and concentration of residual host-cell DNA (hcDNA) to a length of <200 base pairs and <10 ng per dose [35,36] to minimize potential risks such as oncogenic events, autoimmune reactions or transmission of latent viruses and other agents [37–39]. Implementing a nuclease digestion step at different stages of the DSP, effectively addresses this requirement. For viral vector processes this is typically implemented before harvest and clarification. The pre-clarification nuclease treatment allows an incubation at 37 °C which is an ideal temperature for common nucleases resulting in more effective DNA digestion. This reduces the viscosity of the cell culture broth and facilitates the filtration [40], which was also shown in our DoE. Our findings indicate that a nuclease concentration range of 60–80 U•mL^{-1} is optimal, with higher concentration not further reducing DNA levels. Given the cost implications of nuclease use ant its role as a process-

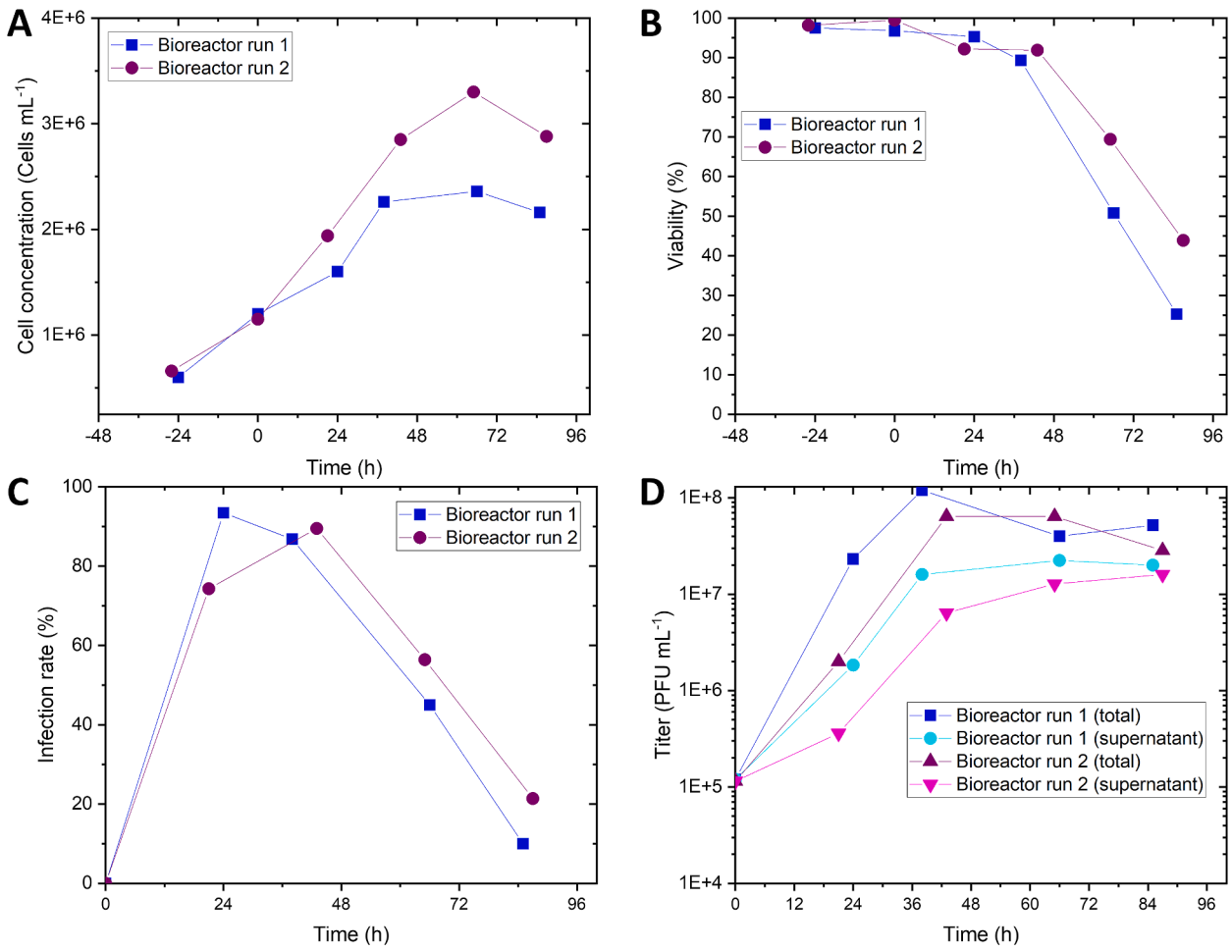

Fig. 3. Upstream data of ORFV production batches. (A) Cell concentration, (B) viability, (C) infection rate (cherry-positive cells), and (D) ORFV titer for the two 6 L bioreactor runs. Time of infection = 0 h. Harvest was performed at three different times: 40, 70, and 90 h (±4h for each) post-infection for runs 1 and 2, respectively.

related impurity to be removed during the subsequent DSP steps [41], it is prudent to use the lowest effective concentration and shortest feasible incubation time. Although literature reports various conditions for nuclease treatment, including the use of Benzonase and Denerase® in different concentration ranges, temperatures, and incubation times, there is no universally accepted standard, underscoring the need for processes-specific optimization. Interestingly, nuclease addition did not negatively impact ORFV titers.

4.3. Filter screening with nuclease treatment

To achieve a comprehensive understanding of optimal conditions for ORFV recovery, it was crucial to conduct a thorough analysis of various critical factors, including bioreactor performance, ORFV yield, turbidity levels, DNA concentration, and filter capacity. Utilizing the automated high-throughput Ambr® Crossflow system, enabled the rapid completion of 168 filtration experiments, significantly accelerating the process. The collated data, depicted in Fig. 5, offers a concise overview of how different harvest times and nuclease treatments impact these parameters, guiding the selection of the most effective harvesting and filtration strategies.

An analysis of the bioreactor data preliminarily suggested the advantages of an earlier TOH due to lower levels of impurities. This observation was corroborated by turbidity measurements which demonstrated more substantial reductions in turbidity when nuclease treatment where applied, particularly for TOH 2 and 3. However, nuclease treatment initially increased turbidity, likely due to fragmentation of large nucleic acid aggregates into finer particle, enhancing the filterability of the broth by reducing its viscosity [42]. Despite similar turbidity reductions for TOH 2 and 3, the final turbidity was noticeably higher for TOH 3, attributed to its elevated starting levels. Consequently, opting for an earlier harvest not only mitigates DSP strain but also balances between maximizing ORFV yield and managing impurity levels, positioning TOH 2 as a good compromise. Achieving adequate turbidity reduction necessitates a dual-stage filtration process, potentially further optimized by selecting lower final pore sizes for the final filter stage. However, given ORFVs considerable particle size, excessively small pore sizes could hinder virus recovery, emphasizing the need for a balanced approach that carefully considers the interplay between turbidity reduction and yield optimization.

Optimizing the TOH was crucial for enhancing ORFV recovery. Later TOH proved advantageous to achieve higher ORFV titers (Fig. S4) and, consequently, the yield in the filtrate. However, transitioning from TOH 2 to TOH 3 did not yield further enhancements, which is consistent with the bioreactor data showing ORFV titers plateau after a certain growth phase. This plateau likely occurs as cell viability decreased over time, leaving a substantial portion of ORFV particles intracellular and unreleased from the host cell to form extracellular virions. The cell death process likely makes these intracellular ORFVs accessible, similar to the release mechanism triggered by freeze–thaw cycles, representing a method of cell lysis which is not suited for large scale production. This underlines the potential of exploring alternative lysis methods or timing the harvest to coincide with natural decreases in cell viability to optimize yield without compromising filter capacity. Furthermore, selecting

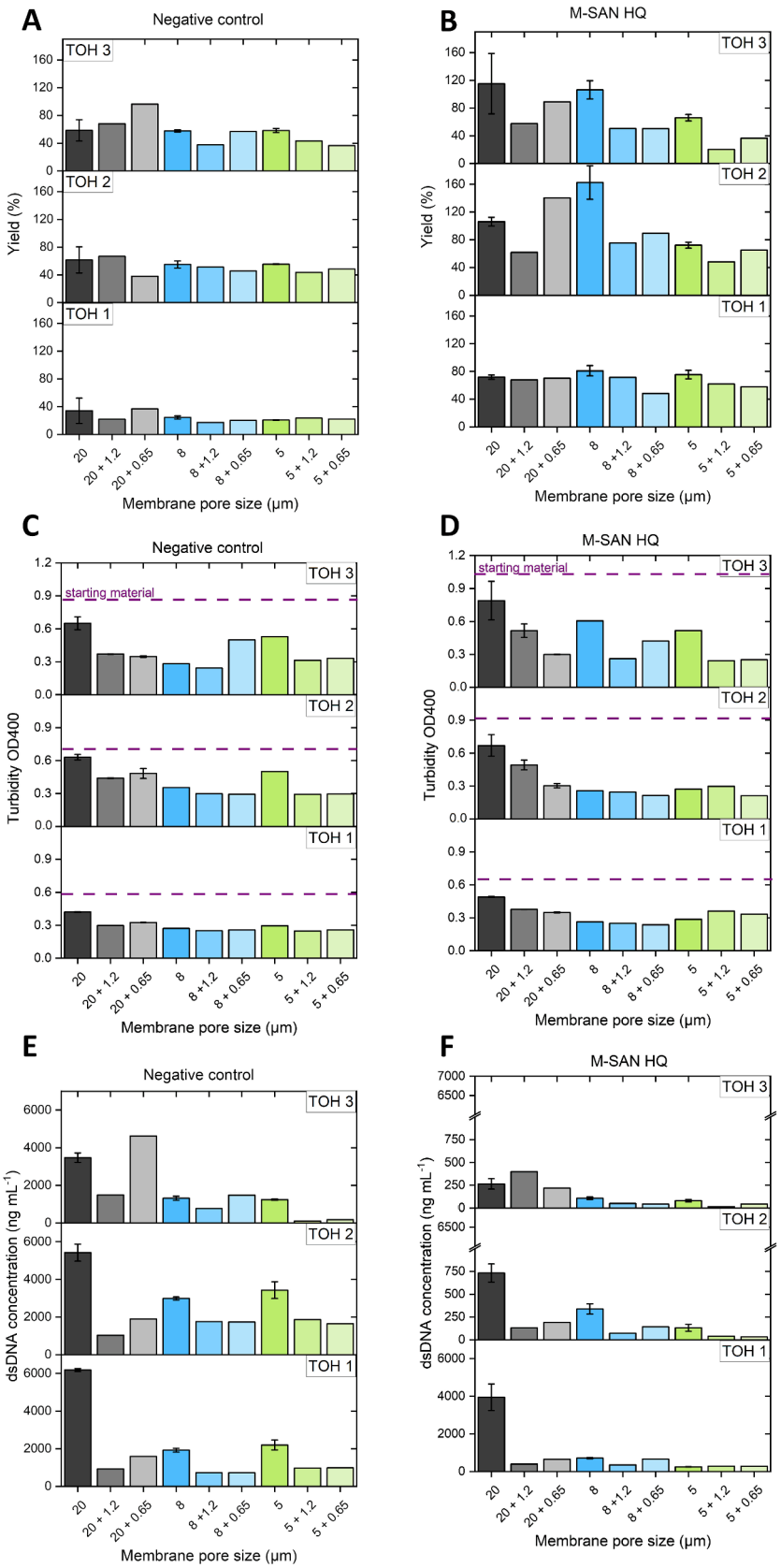

Fig. 4. Filter screening at different times of harvest. ORFV yield, turbidity at OD400, and dsDNA concentration after clarification with Sartopure® PP3 membranes of different pore sizes (A, C, E) without nuclease treatment (negative control) or (B, D, F) with M-SAN HQ treatment. The filtration was performed after three different times of harvest (TOH), which were 40, 70, and 90 h (±4h for each) post-infection.

Table 4
Filter capacities and maximum pressure reached for the filtrations using the Sartopure® PP3 filters. Filtration was targeted to be performed until approximately 1 bar, for filtrations with maximum pressure indicated below 1 bar filtration was stopped earlier due to limited available cell culture material. The values were rounded to whole numbers.

	Membrane pore size (μm)	TOH 1		TOH 2		TOH 3	
		Capacity ($L \bullet m^{-2}$)	Max. pressure (bar)	Capacity ($L \bullet m^{-2}$)	Max. pressure (mbar)	Capacity ($L \bullet m^{-2}$)	Max. pressure (mbar)
Negative control	20	>181	670	174 ± 1	1200	>81 ± 14	560
	20 + 1.2	101.5	945	>108	710	79	1300
	20 + 0.65	>110	555	>107	400	>115	433
	8	112 ± 3	1025 ± 7	98 ± 2	1050 ± 70	79	1175 ± 35
	8 + 1.2	>113	358	>111	340	>98	322
	8 + 0.65	>112	281	>108	430	>95	33
	5	76 ± 2	1273 ± 310	56 ± 15	1088 ± 85	41 ± 5	1118 ± 126
	5 + 1.2	>112	270	>91	500	>111	260
	5 + 0.65	>114	380	>94	300	>96	35
M-SAN HQ	20	>174 ± 3	65 ± 7	142 ± 5	1000	106 ± 1	1260
	20 + 1.2	84	1020	>104	850	>115	750
	20 + 0.65	87	1050	80	1300	121	950
	8	124	1106 ± 8	106	990 ± 14	65 ± 1	1175 ± 106
	8 + 1.2	>117	400	>113	570	>78	520
	8 + 0.65	>118	60	>116	580	>77	620
	5	71 ± 19	1134 ± 31	41 ± 3	1105 ± 122	41 ± 23	1150 ± 58
	5 + 1.2	>112	350	>94	230	>94	240
	5 + 0.65	>113	60	>92	300	>96	380

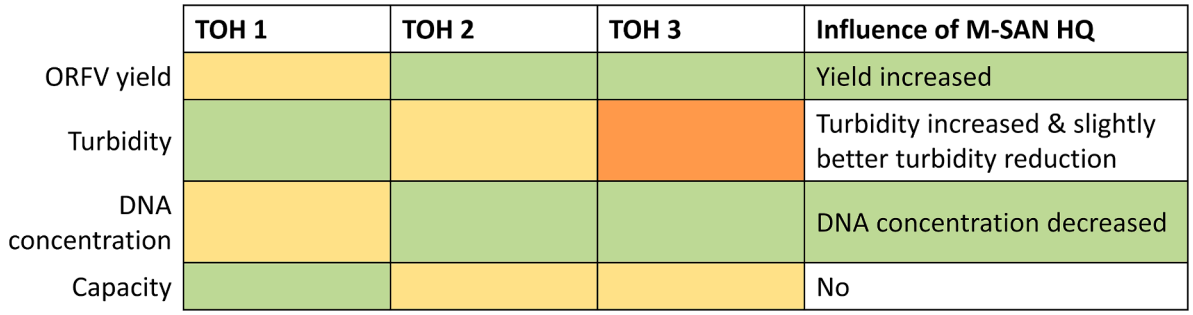

Fig. 5. Summary of the time of harvest (TOH) choice and use of a nuclease. Influence of the time of harvest (TOH) which was 40, 70, and 90 h (±4h for each) post-infection on the aim to achieve a high ORFV yield, a low final turbidity, a low DNA concentration in the filtrate, as well as a high filter capacity. The influence of using M-SAN HQ on these four responses was additionally evaluated. Color code: green = advantageous/good, yellow = medium/ok, and red = disadvantageous to achieve the desired results of the analyzed factors. (For interpretation of the references to color in this figure legend, the reader is referred to the web version of this article.)

larger membrane pore size for primary clarification was found to increase ORFV recovery, suggesting that it allows for the passage of ORFV particles, that are in aggregates or associated to cell debris. Remarkably, secondary filtration with a smaller pore size (0.65 μm) often led to higher ORFV recoveries, however, these differences were rather small and the limited number of replicates does not allow definitive conclusions. Nuclease treatment notably enhanced the recovery of ORFV particles in the filtrate. We hypothesize that ORFV particles may bind to cell fragments and DNA, potentially forming large aggregates that are too big to pass through the filter. The fragmentation of DNA by the nuclease activity, likely disperses these aggregates allowing more ORFV particles to be separated and subsequently pass through the filter and be recovered in the filtrate. Thus, the nuclease treatment not only reduces DNA concentration but also significantly improves the efficiency of ORFV recovery.

Regarding DNA concentration in the filtrate, employing filters with a smaller membrane pore size proved to be more effective in retaining DNA fragments. As expected, the nuclease treatment significantly lowered the DNA concentration in the filtrate, optimizing the purification process. Interestingly, later harvesting times resulted in reduced DNA concentration, a finding that might seem counterintuitive at first glance given the anticipation of increased host cell DNA in the supernatant as cell viability declines. This phenomenon could be attributed to the formation of larger DNA aggregates at elevated DNA concentrations, which are more efficiently retained by the filter membrane. This observation was, however, not uniformly evident across all controls, suggesting a nuanced interplay between DNA concentration, aggregate formation, and filtration efficacy.

The filter capacity could be determined accurately for primary clarification, whereas or secondary filtration only minimum values were obtained, due to shortage of primary filtrate preventing the filters from reaching 1 bar. Nevertheless, these assessments indicate that a scale-up to a 200 L batch using Sartopure® PP3 filters is feasible, requiring fewer 30″ filter capsules than the initial estimates with Cytiva filters suggested. Given that filter capacity diminishes with later TOH, opting for an earlier harvest could lead to the use of fewer filter capsules, optimizing both cost and efficiency.

In our study, TOH 2 was identified as an optimal compromise for maximizing ORFV yield and filter capacity, while minimizing turbidity and DNA concentration. A combination of 5 or 8 μm for primary and 1.2 or 0.65 μm for secondary filtration stages deemed effective. Additionally, the use of M-SAN HQ significantly improved both, ORFV recovery and DNA clearance. To address the functionality and quality of the viral product, we employed FACS titer measurements to quantify virus yield. This method not only provides us with a quantitative assessment of the viral particles but also offers indirect insights into the quality and

functionality of the recovered ORFV. Observing the virus's ability to infect and replicate within cells serves as a practical in vitro measure of its functionality. It's important to note that we did not continuously monitor host cell protein levels during our study, as filtration has not shown any noticeable impact on these levels (see Fig. S1A + B), nor was any change anticipated. Our findings on the ORFV clarification process likely have broader implications beyond Poxviruses such as Vaccinia Virus, Canarypox virus or Fowlpox virus, potentially benefiting the production processes of Adenoviruses, Adeno-Associated Viruses (AAVs), and Lentiviruses. These vectors, often produced in HEK293 suspension cells and undergoing similar downstream processing challenges, could see improvements in filtration efficiency and reductions in host cell DNA (hcDNA) levels through the application of nuclease treatment combined with two stage filtrations. This approach not only promises to enhance clarification but also addresses a common challenge across viral vector production, highlighting the value of our study's insights for a wider range of viral therapeutics and vaccines. For the scale-up of a 200 L production, utilizing Maxicaps® MR (30″ capsules) equipped with Sartopure® PP3 membranes is a practical approach. Calculations, incorporating a 25 % safety margin, estimate the need for about 6.13 m^2 and less than 2.75 m^2 of membrane area for primary and secondary clarification stages, respectively, for a TOH 2 200 L batch. This setup translates to an efficient operation with four capsules needed for the primary clarification and three capsules for the secondary clarification, facilitating streamlined parallel processing for large-scale production.

5. Conclusion

The increasing number of studies of ORFV-based vectors for therapeutic or vaccine applications necessitates scalable production methods to meet clinical trial demands and market delivery. Transitioning from adherent Vero cell processes to a HEK cell suspension process, required extensive optimization of the clarification process, central to this study. Through a DoE approach, M-SAN HQ in concentration of 60–75 $U \bullet mL^{-1}$, at 37 °C for 4 h emerged as the most efficient for DNA reduction. Screening various filter materials and membrane pore sizes pinpointed polypropylene-based filters polypropylene-based filters as optimal despite challenges in filter capacity for large-scale operations. Employing the Ambr® crossflow for high-throughput testing, we established that harvest timing and nuclease application significantly enhance ORFV yields and purity, suggesting a scalable clarification method for ORFV and potentially other large viruses.

Declaration of generative AI in scientific writing

During the preparation of this work the authors used ChatGPT (OpenAI) in order to improve language, grammar and readability of the manuscript. After using this tool, the authors reviewed and edited the content as needed and take full responsibility for the content of the publication.

Funding

This research was supported in part by the Institutional Strategy of the University of Tübingen (Deutsche Forschungsgemeinschaft ZUK63), the EXIST Forschungstransfer of the German Ministry for Economic Affairs and Energy, which is co-financed by the European Social Fund.

CRediT authorship contribution statement

Felix Pagallies: Writing – original draft, Visualization, Methodology, Investigation, Formal analysis. **Jennifer J. Labisch:** Writing – original draft, Visualization, Formal analysis, Data curation. **Malgorzata Wronska:** Writing – review & editing, Investigation. **Karl Pflanz:** Writing – review & editing, Conceptualization. **Ralf Amann:** Writing – review & editing, Supervision, Resources, Project administration, Funding acquisition, Conceptualization.

Declaration of competing interest

The authors declare the following financial interests/personal relationships which may be considered as potential competing interests: Ralf Amann reports financial support was provided by University Hospitals Tubingen. Amann Ralf reports a relationship with Prime Vector Technologies that includes: employment and equity or stocks. Ralf Amann is a co-founder of Prime Vector Technologies (PVT). PVT aims to develop vaccines based on Orf virus. If there are other authors, they declare that they have no known competing financial interests or personal relationships that could have appeared to influence the work reported in this paper.

Data availability

Data will be made available on request.

Acknowledgements

We would like to kindly thank Marius Iseke for assistance with the Ambr® crossflow filtration experiments. Many thanks go as well to Jochem Pronk from Batavia Biosciences and Dr. Peter Eiermann from Cytiva for their help with filtration experiments.

Appendix A. Supplementary material

Supplementary data to this article can be found online at https://doi.org/10.1016/j.jvacx.2024.100474.

References

[1] Eilts F, Labisch JJ, Orbay S, Harsy YMJ, Steger M, Pagallies F, et al. Stability studies for the identification of critical process parameters for a pharmaceutical production of the Orf virus. Vaccine 2023;41(32):4731–42. https://doi.org/10.1016/j.vaccine.2023.06.047.
[2] Lacek K, Bauer B, Bieńkowska-Szewczyk K, Rziha H-J. Orf virus (ORFV) ANK-1 protein mitochondrial localization is mediated by ankyrin repeat motifs. Virus Genes 2014;49(1):68–79. https://doi.org/10.1007/s11262-014-1069-5.
[3] Eilts F, Steger M, Pagallies F, Rziha H-J, Hardt M, Amann R, et al. Comparison of sample preparation techniques for the physicochemical characterization of Orf virus particles. J Virol Methods 2022;310:114614. https://doi.org/10.1016/j.jviromet.2022.114614.
[4] Spehner D, de Carlo S, Drillien R, Weiland F, Mildner K, Hanau D, et al. Appearance of the bona fide spiral tubule of ORF virus is dependent on an intact 10-kilodalton viral protein. J Virol 2004;78(15):8085–93. https://doi.org/10.1128/JVI.78.15.8085-8093.2004.
[5] Müller M, Reguzova A, Löffler MW, Amann R. Orf virus-based vectors preferentially target professional antigen-presenting cells, activate the STING pathway and induce strong antigen-specific T cell responses. Front Immunol 2022;13:873351. https://doi.org/10.3389/fimmu.2022.873351.
[6] Amann R, Rohde J, Wulle U, Conlee D, Raue R, Martinon O, et al. A new rabies vaccine based on a recombinant ORF virus (parapoxvirus) expressing the rabies virus glycoprotein. J Virol 2013;87(3):1618–30. https://doi.org/10.1128/JVI.02470-12.
[7] Rziha H-J, Büttner M, Müller M, Salomon F, Reguzova A, Laible D, et al. Genomic characterization of Orf virus strain D1701-V (parapoxvirus) and development of novel sites for multiple transgene expression. Viruses 2019;11(2). https://doi.org/10.3390/v11020127.
[8] Reguzova A, Ghosh M, Müller M, Rziha H-J, Amann R. Orf virus-based vaccine vector D1701-V induces strong CD8+ T cell response against the transgene but not against ORFV-derived epitopes. Vaccines (Basel) 2020;8(2). https://doi.org/10.3390/vaccines8020295.
[9] Reguzova A, Fischer N, Müller M, Salomon F, Jaenisch T, Amann R. A novel Orf virus D1701-VrV-based dengue virus (DENV) vaccine candidate expressing HLA-specific T cell epitopes: a proof-of-concept study. Biomedicines 2021;9(12). https://doi.org/10.3390/biomedicines9121862.
[10] Rohde J, Amann R, Rziha H-J. New Orf virus (Parapoxvirus) recombinant expressing H5 hemagglutinin protects mice against H5N1 and H1N1 influenza A virus. PLoS One 2013;8(12):e83802. https://doi.org/10.1371/journal.pone.0083802.
[11] Fischer T, Planz O, Stitz L, Rziha H-J. Novel recombinant parapoxvirus vectors induce protective humoral and cellular immunity against lethal herpesvirus

challenge infection in mice. J Virol 2003;77(17):9312–23. https://doi.org/10.1128/JVI.77.17.9312-9323.2003.
[12] Dory D, Fischer T, Béven V, Cariolet R, Rziha H-J, Jestin A. Prime-boost immunization using DNA vaccine and recombinant Orf virus protects pigs against pseudorabies virus (Herpes suid 1). Vaccine 2006;24(37–39):6256–63. https://doi.org/10.1016/j.vaccine.2006.05.078.
[13] van Rooij EMA, Rijsewijk FAM, Moonen-Leusen HW, Bianchi ATJ, Rziha H-J. Comparison of different prime-boost regimes with DNA and recombinant Orf virus based vaccines expressing glycoprotein D of pseudorabies virus in pigs. Vaccine 2010;28(7):1808–13. https://doi.org/10.1016/j.vaccine.2009.12.004.
[14] Voigt H, Merant C, Wienhold D, Braun A, Hutet E, Le Potier M-F, et al. Efficient priming against classical swine fever with a safe glycoprotein E2 expressing Orf virus recombinant (ORFV VrV-E2). Vaccine 2007;25(31):5915–26. https://doi.org/10.1016/j.vaccine.2007.05.035.
[15] Rohde J, Schirrmeier H, Granzow H, Rziha H-J. A new recombinant Orf virus (ORFV, Parapoxvirus) protects rabbits against lethal infection with rabbit hemorrhagic disease virus (RHDV). Vaccine 2011;29(49):9256–64. https://doi.org/10.1016/j.vaccine.2011.09.121.
[16] Henkel M, Planz O, Fischer T, Stitz L, Rziha H-J. Prevention of virus persistence and protection against immunopathology after Borna disease virus infection of the brain by a novel Orf virus recombinant. J Virol 2005;79(1):314–25. https://doi.org/10.1128/JVI.79.1.314-325.2005.
[17] Rintoul JL, Lemay CG, Tai L-H, Stanford MM, Falls TJ, de Souza CT, et al. ORFV: a novel oncolytic and immune stimulating parapoxvirus therapeutic. Mol Ther 2012;20(6):1148–57. https://doi.org/10.1038/mt.2011.301.
[18] Schneider M, Müller M, Yigitliler A, Xi J, Simon C, Feger T, et al. Orf virus-based therapeutic vaccine for treatment of papillomavirus-induced tumors. J Virol 2020;94(15). https://doi.org/10.1128/JVI.00398-20.
[19] Reguzova A, Sigle M, Pagallies F, Salomon F, Rziha H-J, Bittner-Schrader Z, et al. A novel multi-antigenic parapoxvirus-based vaccine demonstrates efficacy in protecting hamsters and non-human primates against SARS-CoV-2 challenge; 2023.
[20] Rziha H-J, Rohde J, Amann R. Generation and selection of Orf virus (ORFV) recombinants. Methods Mol Biol 2016;1349:177–200. https://doi.org/10.1007/978-1-4939-3008-1_12.
[21] van Vloten JP, Minott JA, McAusland TM, Ingrao JC, Santry LA, McFadden G, et al. Production and purification of high-titer OrfV for preclinical studies in vaccinology and cancer therapy. Mol Ther Methods Clin Dev 2021;23:434–47. https://doi.org/10.1016/j.omtm.2021.08.004.
[22] Lothert K, Pagallies F, Eilts F, Sivanesapillai A, Hardt M, Moebus A, et al. A scalable downstream process for the purification of the cell culture-derived Orf virus for human or veterinary applications. J Biotechnol 2020;323:221–30. https://doi.org/10.1016/j.jbiotec.2020.08.014.
[23] Lothert K, Pagallies F, Feger T, Amann R, Wolff MW. Selection of chromatographic methods for the purification of cell culture-derived Orf virus for its application as a vaccine or viral vector. J Biotechnol 2020;323:62–72. https://doi.org/10.1016/j.jbiotec.2020.07.023.
[24] Lothert K, Harsy YMJ, Endres P, Müller E, Wolff MW. Evaluation of restricted access media for the purification of cell culture-derived Orf viruses. Eng Life Sci 2023. https://doi.org/10.1002/elsc.202300009.
[25] Besnard L, Fabre V, Fettig M, Gousseinov E, Kawakami Y, Laroudie N, et al. Clarification of vaccines: an overview of filter based technology trends and best practices. Biotechnol Adv 2016;34(1):1–13. https://doi.org/10.1016/j.biotechadv.2015.11.005.
[26] Carvalho SB, Silva RJ, Moreira AS, Cunha B, Clemente JJ, Alves PM, et al. Efficient filtration strategies for the clarification of influenza virus-like particles derived from insect cells. Sep Purif Technol 2019;218:81–8. https://doi.org/10.1016/j.seppur.2019.02.040.
[27] Gränicher G, Babakhani M, Göbel S, Jordan I, Marichal-Gallardo P, Genzel Y, et al. A high cell density perfusion process for modified vaccinia virus Ankara production: process integration with inline DNA digestion and cost analysis. Biotechnol Bioeng 2021;118(12):4720–34. https://doi.org/10.1002/bit.27937.
[28] Buchschacher GL, Wong-Staal F. Development of lentiviral vectors for gene therapy for human diseases. Blood 2000;95(8):2499–504.
[29] Fleming SB, Wise LM, Mercer AA. Molecular genetic analysis of Orf virus: a poxvirus that has adapted to skin. Viruses 2015;7(3):1505–39. https://doi.org/10.3390/v7031505.
[30] Roberts KL, Smith GL. Vaccinia virus morphogenesis and dissemination. Trends Microbiol 2008;16(10):472–9. https://doi.org/10.1016/j.tim.2008.07.009.
[31] Labisch JJ, Bollmann F, Wolff MW, Pflanz K. A new simplified clarification approach for lentiviral vectors using diatomaceous earth improves throughput and safe handling. J Biotechnol 2021;326:11–20. https://doi.org/10.1016/j.jbiotec.2020.12.004.
[32] Meierrieks F, Pickl A, Wolff MW. A robust and efficient alluvial filtration method for the clarification of adeno-associated viruses from crude cell lysates. J Biotechnol 2023;367:31–41. https://doi.org/10.1016/j.jbiotec.2023.03.010.
[33] Prashad M, Tarrach K. Depth filtration: cell clarification of bioreactor offloads. Filtr Sep 2006;43(7):28–30. https://doi.org/10.1016/S0015-1882(06)70950-8.
[34] European Pharmacopoeia, Chapter 5.2.3. Cell substrates for the production of vaccines for human use.
[35] World Health Organization. WHO expert committee on biological standardization. Geneva, Switzerland; 2003.
[36] US Food and Drug Administration. Guidance for industry: characterization and qualification of cell substrates and other biological materials used in the production of viral vaccines for infectious disease indications. Rockville, USA; 2010.
[37] Graham FL, Smiley J, Russell WC, Nairn R. Characteristics of a human cell line transformed by DNA from human adenovirus type 5. J Gen Virol 1977;36(1):59–74. https://doi.org/10.1099/0022-1317-36-1-59.
[38] Sheng-Fowler L, Lewis AM, Peden K. Issues associated with residual cell-substrate DNA in viral vaccines. Biologicals 2009;37(3):190–5. https://doi.org/10.1016/j.biologicals.2009.02.015.
[39] Sheng L, Cai F, Zhu Y, Pal A, Athanasiou M, Orrison B, et al. Oncogenicity of DNA in vivo: tumor induction with expression plasmids for activated H-ras and c-myc. Biologicals 2008;36(3):184–97. https://doi.org/10.1016/j.biologicals.2007.11.003.
[40] Moleirinho MG, Silva RJS, Alves PM, Carrondo MJT, Peixoto C. Current challenges in biotherapeutic particles manufacturing. Expert Opin Biol Ther 2020;20(5):451–65. https://doi.org/10.1080/14712598.2020.1693541.
[41] Wolff MW, Reichl U. Downstream processing of cell culture-derived virus particles. Expert Rev Vaccines 2011;10(10):1451–75. https://doi.org/10.1586/erv.11.111.
[42] Hebben M. Downstream bioprocessing of AAV vectors: industrial challenges & regulatory requirements. Cell Gene Therapy Insights 2018;4(2):131–46. https://doi.org/10.18609/cgti.2018.016.